Killing bacteria by Faradaic processes through MoO_x - hydroxyapatite nano-platforms

*Juan M. Sieben[a§], Damián Placente[a§], Mónica D. Baldini [b], Juan M. Ruso[c], Paula V. Messina [a]**

(a) INQUISUR – CONICET, Department of Chemistry, Universidad Nacional del Sur, B8000CPB, Bahía Blanca, Argentina. (b) Department of Biology, Biochemistry and Pharmacy, Universidad Nacional del Sur, B8000ICN, Bahía Blanca, Argentina. (c) Soft Matter and Molecular Biophysics Group, Department of Applied Physics, University of Santiago de Compostela, 15782 Santiago de Compostela, Spain

* Author to whom correspondence should be addressed. Tel: +54 291 4595159. Fax: +54 291 4595160. Electronic mail: pmessina@uns.edu.ar.

§ Juan M. Sieben and Damian Placente contributed equally to this work.

ABSTRACT. Following the secular idea of *"restitutio ad integrum",* regeneration is the pursued option to restore bone lost after a disease, injury or infection. Construction of bone grafts that can simultaneously induce regeneration and exert antibiotic capacity represent a huge scientific challenge. This study is a framework proposal for understanding the antimicrobial effect of bone mimetic networks based on MoO_x-hydroxyapatite nanoparticles on basis of their electroactive behaviour. Through steady cyclic voltammetry and chronoamperometry measurements, the electron transference capacity of HA and HA/MoOx nano-platforms electrodes (nano-HAE, nano-HA/MoOx(II)E and nano-HA/MoOx(III)E) was determined in the absence and in the presence of pathogenic organisms: *Pseudomona aeruginosa* and *Staphylococcus aureus*. Faradaic processes are confirmed and related to the switch of MoO_4^{2-} /PO_4^{3-} in the original hexagonal nano-HA crystal lattice and to the extent of OH-vacancies, V_{OH} defects, that act as electron acceptors. Microscopic analysis of bacteria's ultrastructure shows a disruptive effect upon direct contact with the materials that was not observed in the presence of prokaryotic cells, evidencing that a type of EET process exists and alters the function of their cytoplasmic membranes accelerating their death. Our findings provides strong quantitative support for an antibiotic mechanism based on the enhancement of electron transfer processes between microorganism and phosphates based materials, and provides insights into the use of electroactive modify biomaterials to combat implant-associated orthopaedic infections.

1. INTRODUCTION

Bone tissue infections, such as osteomyelitis, septic arthritis, and prosthetic joint infections (PJIs), continue to represent the worst complications in trauma, presenting one of the greatest challenges in orthopaedic surgery.[1, 2] To combat them, conventional

therapies rely on oral biocidal substances, with an effective success rate only of 22 - 37 % due to bacterial resistance, unfavourable dose-efficacy ratio, and the toxicity of antibiotics.[2, 3] As a result, post-operative extra complications arise, exposing patients to severe pain and numerous risks.[2] In such scenery, two main novel perspectives have emerged to conquer the war against microbial contaminations. Biochemical methodologies that include local controlled release of cytokines[4] or antibiotic peptides[5-7] from drug-eluting implants to stimulate the body's natural defence system and, biophysical tactics, which provides a surface that, after regulating the characteristics of substrate / cell interactions, avoid infection after direct contact. [1, 8]

The second line of attack, selected by us, exploit the fact that mammalian cells and tissues are capable of detecting physical, [9] magnetic, [10] and electrical[11] stimuli from the substrate and then translate them into biochemical and biological responses. In this sense, we have successfully adapted the chemical composition, degree of crystallinity, hydrophilicity and morphology of bone mimetic networks based on rod-like hydroxyapatite nanoparticles, nano-HA.[12-15] Further, we show that the insertion of molybdenum, Mo, an essential trace element, into the non-stoichiometric calcium-deficient hydroxyapatite network generates intrinsic electronic point defects that, acting as electron acceptors, stimulate the biological redox state of the materials and promote pathogenic microorganisms' death after direct contact. [15]

Actually, there are strategies that applied the charge transfer theory of killing bacteria based on the direct contact with metallic semiconductors nano-platforms.[16-19] To the best of our knowledge, the theory of charge transfer associated with antibiotic activity has not been extended to phosphate-based ceramic materials, as the ability of electroactive ceramic nanostructures to kill microorganisms directly from implant bone tissue has been largely overlooked. In this article, we validate a mechanism by which bacteria transfer

electrons to MoO_x-hydroxyapatite nano-platforms. Antibacterial activity were confirmed against drug-resistance strains responsible to clinical bone infections: *Staphylococcus aureus* and *Pseudomona aeruginosa*. We have hypothesized that the electronic transference of the bacterial metabolic circuit alters the function of the prokaryote cytoplasmic membrane to the point of inducing decease. The mechanism is not operative with eukaryotic cells, maintaining the biocompatibility of the original nano-HA.[15] Our findings highlight the importance and the need for fine-tuning electronic communications between biomaterial interfaces and biological units, and support their use in advanced tactics to combat implant-associated orthopaedic infections.

2. EXPERIMENTAL

2.1 Reagents

Triblock poly(ethylene glycol)-poly(propylene glycol)-poly(ethylene glycol) copolymer Pluronic® F-127 ($EO_{102}PO_{70}EO_{102}$, CAS n° 9003-11-6, BioReagent, Sigma - Aldrich); polyethylene glycol (20) sorbitan monostearate (Tween® 60, CAS n° 9005-67-8, Sigma - Aldrich); sodium phosphate tribasic dodecahydrate ($Na_3PO_4 \cdot 12H_2O$, CAS n° 10101-89-0, Sigma - Aldrich); calcium chloride ($CaCl_2$, CAS 10043-52-4, Sigma - Aldrich); phosphomolybdic acid hydrate ($H_3[P(Mo_3O_{10})_4] \cdot xH_2O$, x = 28[15], CAS n°51429-74-4, Sigma – Aldrich); phosphate buffer saline (PBS tablets, Na_2HPO_4 / NaH_2PO_4, Sigma - Aldrich); potassium ferricyanide (III) ($K_3Fe(CN)_6$, CAS n° 13746-66-2, Merk); potassium ferrocyanide (IV) trihydrate ($K_4Fe(CN)_6 \cdot 3H_2O$, CAS n° 14459-95-1, Merk); L-Ascorbic acid redox probe ($C_6H_8O_6$, CAS n°A92902 Sigma - Aldrich); Dopamine hydrochloride ($C_8H_{12}ClNO_2$, CAS n° 62-31-7 Sigma - Aldrich), Iron(II) sulfate heptahydrate ($Fe(II)SO_4.7H_2O$, CAS n° 7782-63-0 Sigma- Aldrich), - Iron(III) sulfate hydrate ($Fe_2(III)(SO_4)_3 \cdot xH_2O$, CAS n° 15244-10-7 Sigma- Aldrich), Glucose

monohydrate ($C_6H_{12}O_6 \cdot H_2O$, CAS n° 14431-43-7 Sigma- Aldrich), and ethanol (EtOH, CAS n° 64-17-5, Sigma – Aldrich) were used without further purification. For solutions preparation, only Milli-Q water was used.

2.2 MoO_x -hydroxyapatite nano-platforms

Rod-like hydroxyapatite nanoparticles, nano-HA, and its MoO_x - derivatives denoted as (nano-HA/MoO_x (II), 0.48 $mmol_{Mo}$ / g_{HA}) and (nano-HA/MoO_x (III); 4.30 $mmol_{Mo}$ / g_{HA}) were prepared and characterized as previously described by Placente *et al.*[15] In the HA/MoO_x (II) specimen, phosphate $(PO_4)^{3-}$ ions are substituted by the metal complex molybdate $(MoO_4)^{2-}$ into the hexagonal lattice, crystallographic space group $P6_3/m$, of calcium deficient nonstoichiometric hydroxyapatites, $Ca_{10-x}(HPO_4)_x(PO_4)_{6-x}(OH)_{2-x}$.[15] In HA/$MoO_x$ (III), a second phase of powellite ($CaMoO_4$) was detected.[15] Topographical characterization was performed using a field emission scanning electron microscopy (FE-SEM) ZEISS ULTRA PLUS coupled to an X-ray energy-dispersive (EDX) spectrophotometer that enables elemental chemical microanalysis. Images were acquired with a secondary electron detector (In lens) operated at an accelerating voltage (EHT) of 3.00 kV and at a working distance (WD) resolution of 2.1 nm. Local compensation of charge was achieved by injecting nitrogen gas. To evaluate the asymmetry of the roughness profile about the mean line, the profile skewness (R_{sk}) and kurtosis (R_{ku}) were computed.[20] Two randomly chosen areas (one in a central position and one at 1.5 mm from the outer edge) on each micrographs were taken. 3D surface plots, (R_{sk}) and (R_{ku}) parameters were obtained using the image visualization software Image J, 1.34 s, NIH Image, USA with an uncertainty of 5 %. [21]

The electric potential in the sliding plane adjacent to the nano-HA/MoO_x platforms was measured with a Malvern Zeta Sizer Nano (ZS90) with a He-Ne laser (λ = 633 nm).

Malvern's software provides the Zeta potential (ζ) measurements from electrophoretic mobilities (μE), using the Henry equation. [22] Experimentally, all samples (0.2 mg mL^{-1}) were diluted with filtered hydration medium (PBS, pH = 7.4) to an appropriate counting rate prior to analysis; reported values were the result of ten independently determinations. Ionic concentration released from nano-HA/MoO_x platforms after 10 days of degradation in PBS (pH = 7.4) at 37°C was determined as previously described.[15]

2.3 Electrochemical assessment of bacterial interaction with nano-HA/MoO_x platforms

2.3.1 Pseudomona aeruginosa / Staphylococcus aureus culture. Antimicrobial effects of nano-HA and nano-HA/MoO_x platforms were performed against two bacterial strains representing a clinically relevant spectrum of microorganisms.[23] Gram-negative, *Pseudomona aeruginosa* (ATCC 27853) and, Gram-positive, *Staphylococcus aureus* (ATCC 29213) bacteria were isolated and stored at Microbiology Chair, Department of Biology, Biochemistry and Pharmacy of the Universidad Nacional del Sur, Argentina.

An inoculum of *Pseudomona aeruginosa* was prepared and grown overnight at 37°C to ensure an exponential progress before their use. Then, the necessary volume to achieve a turbidity equivalent to 0.5 Mc Farland scale (determined by a 0.08 optical density measured at 550 nm) was taken and placed in test tubes with 15 mL of standard nutritive broth (Sigma-Aldrich, CAS no. 70122). The same procedure was performed for the *Staphylococcus aureus* strain. In order to quantify the bacterial concentration, the properly dilutions were seeded by the overturned agar technique to obtain plates that had between 30 and 300 colonies using a plate count agar (PCA, Merck, no. 1054630500). Following, the number of colony-forming units (CFU) per millilitre was quantified, being 4 x 10^6 CFU / mL for *Pseudomona aeruginosa*, and 7 x10^6 CFU / mL for *Staphylococcus aureus* strain.

2.3.2 Working electrodes preparation. Four different types of 0.07 cm^2 geometric area electrodes were prepared and then placed in contact with each bacteria strain dispersion; that is, an unmodified glassy carbon electrode (GCE) used as control, and nano-platforms modified electrodes (nano-PEs) that contains nano-HA, nano-HA/MoOx (II) and nano-HA/MoOx (III) specimens deposited on the GCE surface. For the preparation of nano-PEs, 20 µL of an absolute ethanol material dispersion (20 mg / mL) was deposited on the glassy carbon electrode surface. After the deposited dispersion was air dried, a drop (≈ 5 µL) of 0.05 % w/v Nafion™ 117 containing solution (Sigma – Aldrich, CAS No.: 31175-20-9) was added. All electrodes were sterilized with UV light throughout 3 hours in a laminar flow cabinet, and remain there until they are brought into contact with the bacterial culture.

2.3.3 Bacterial surface adsorption on electrodes. To achieve the bacterial adsorption on the working electrode surfaces, 1.5 mL of bacterial culture was added to test tubes, previously sterilized in an autoclave at 120 °C along 30 min. Next, electrodes prepared accordingly to the previously described procedure were introduced so that only it surface remained in contact with the bacterial culture for a period of 72 h at room temperature (RT). The whole process was carried out in a laminar flow cabinet to avoid external contamination.

2.3.4 Bacterial surface adsorption quantification. The surface adsorption capacity of *Pseudomona aeruginosa* and *Staphylococcus aureus* strains on GCE surface and on the nano-PEs that contained a film of superficial Nafion was quantified. To this, electrodes were placed in contact with 1.5 mL of 0.5 Mc Farland bacterial culture in exponential growth throughout 72 hours at RT. Then, bacteria were removed applying the surface swab method [24] with a sterile cotton swabs on behalf of 1 minute. Bacteria were recovered from the swab by mechanical agitation (Vortex) along 2 minutes in a diluent medium (3

mL of peptone water solution containing 1% w/v peptone and 0.5 % w/v NaCl). The obtained bacteria dilutions were then seeded using the overturned agar technique, in order to obtain plates with between 30 and 300 colonies, using a plate count agar (PCA, Merck, no. 1054630500). Amount of adsorbed bacteria in each electrode was reported as colony-forming units per electrode geometric area, CFU / cm^2 and summarized in **table 1**. Each experiment was performed in triplicate; the normality and homoscedasticity of the data set were verified, and media values were compared by means of the T-Test [25] with a significance level of 0.05. No significant differences were found between the adsorption of both groups for each bacterial strain on electrodes with and without Nafion film.

- Please insert table 1, here -

2.3.5 Steady cyclic voltammetry and chronoamperometry tests.

The impedance of bare GCE and nano-PEs were measured against the redox conversion of different surface sensitive probes: $[Fe(CN)_6]^{-3/-4}$, ascorbic acid and dopamine, 10 mM in phosphate buffer (PBS, 0.1 M potassium phosphate, pH = 7.2). Electron transfer characteristics of GCE and nano-PEs after bacterial strains adsorption, was evaluated against ($[Fe(CN)_6]^{-3/-4}$, 10 mM) in phosphate buffer (PBS, 0.1 M potassium phosphate, pH = 7.2) in an unstirred solution. Redox probe is usually employed to evaluate electronic transference in biomimetic systems[26] and the effects on growth and morphology of bacteria were negligible at ferricyanide concentrations inferior to 25.0 mM. [27] Application of cyclic voltammetry to living bacteria required a limited potential range to prevent harmful oxidizing or reducing conditions; it was confirmed that under our operational conditions bacteria strain were not affected by exposure to working potentials between - 0.55 and 1 mV versus saturated calomel electrode (SCE). Measurements were performed in a 1 mL capacity three-electrode electrochemical cell, containing a working electrode (GCE; nano-PEs), a counter electrode (platinum wire) and a reference electrode

(SCE, + 0.241 vs. NHE), **scheme 1a**. Steady cyclic voltammograms (CV) were recorded in a VersaSTAT 3 Princeton Applied Research potentiostat / galvanostat at RT by the application of different scanning speeds ranging from 10 to 500 mV/ s. The extracted peak potential values (both for oxidation and reduction processes namely E_{ox} and E_{red} respectively) and the voltammetric peak separation (ΔE_p) were investigated. The scan rate dependence with the peak height for the anodic and cathodic branches of the voltammograms was evaluated by the Randles-Ševčik equation: [28]

$$I_p = 2.687\ x\ 10^5 ACn^{3/2}(Dv)^{1/2} \quad (1)$$

where, I_p, is the peak current (A), A is the electroactive area (cm^2), C is the concentration of the electroactive specie (mol / cm^3), n is the number of exchanged electrons, D is the diffusion coefficient (cm^2 / s) and ν is the scan rate (V/ s), respectively. Then, heterogeneous rate constant (k^0) was computed as follows:

$$k^0(cm/s) = \sqrt{\left(\frac{\pi DnF\nu}{RT}\right)}\psi \quad (2)$$

where, F, R and T have their usual significance, while Ψ is a dimensionless charge transfer parameter that depends on the peak separation (ΔE_p) and ν is the scan rate of the cyclic voltammetry experiments.

Faradaic processes - which are due to electron transfer events and are the current component of interest - occurring at GCE and nano-PEs in contact with bacterial strains, was monitored as a function of time at fixed potential (0.2 V) by the chronoamperometry test. Chronoamperograms were recorded throughout 24 hours at RT checking the redox conversion of $Fe^{+2/+3}$ probe in a PBS solution containing 50 µM of ferrous sulfate, 100 µM of ferric sulfate and 100 mM Glucose. All measurements were performed in triplicate.

2.3.6 Bacterial ultrastructure inspection. Bacterial ultrastructural inspection was performed by transmission electron microscopy (TEM) observations. For this experiment, 1 mL of bacterial dispersion after 48 h of material contact was taken, fixed

with glutaraldehyde solution (Grade I, 25% in H_2O solution, CAS N°111-30-8, Sigma-Aldrich), after brief washing in PBS buffer, the fixed specimens were dehydrated in an ascending graded ethanol (EtOH) series. For embedding, the EtOH was replaced stepwise by a polyhydroxy-aromatic acrylic resin (LR White), starting at a resin:EtOH ratio of 1:2, followed by 1:1, 2:1, and three times in resin only, each for 30 min. Finally, samples were embedded in resin at 60 °C. The hardened resin was then cut into ultrathin sections (40 - 60 nm), transferred onto cupper supports of 2000 mesh, properly stained with a 2 % w/v uranyl acetate water solution (pH 4.2 to 4.5) and observed in a Philips CM-12 transmission electron microscope operated at 120 kV provided with a digital camera MEGA VIEW-II DOCU in a bright field.

2.4 Statistical analysis

All quantitative assessments were taken at least in triplicate, and results are expressed as mean ± standard deviation (SD). Statistical analysis of data was realized by one factor analysis of variance (ANOVA). Student's T-test and probability values below 0.05 ($p < 0.05$) were considered as a significantly difference.

3. RESULTS AND DISCUSSION

3.1 Nano-HA and nano-HA/MoO_x substrates: physical-chemical cues in bacterial progression.

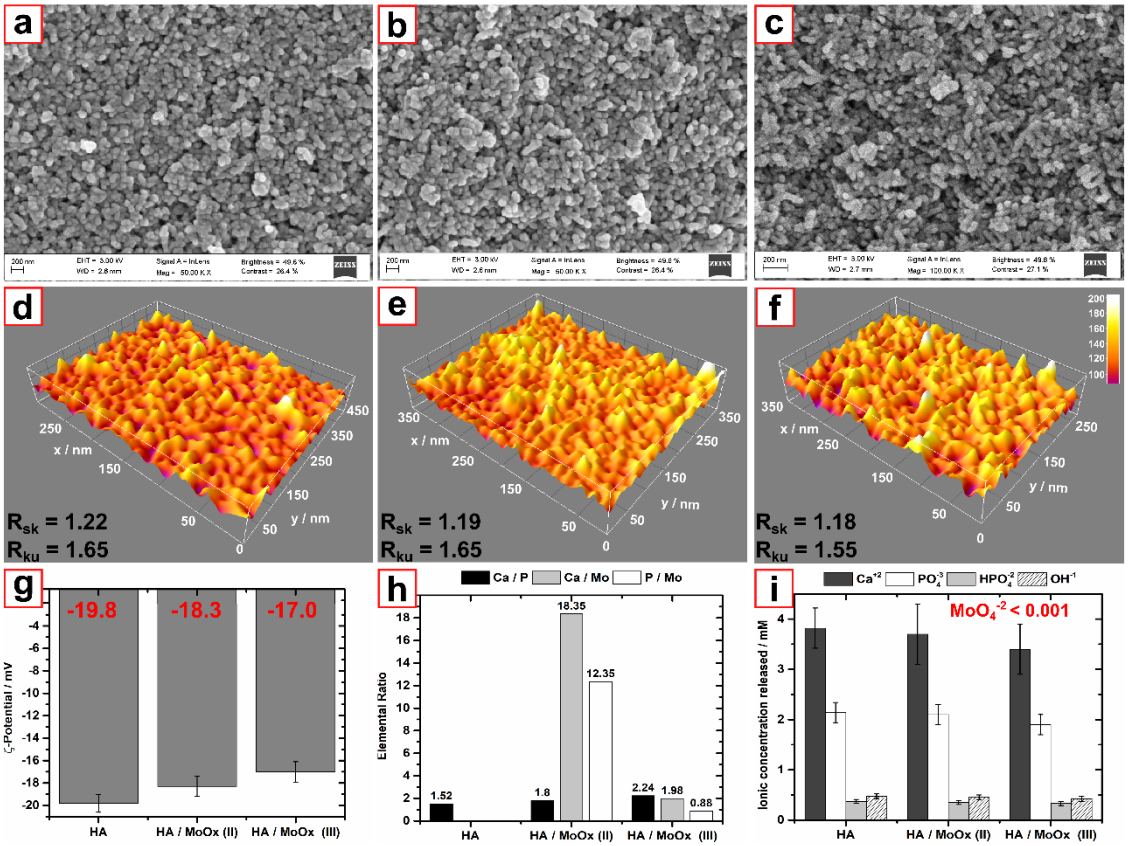

Figure 1. FE-SEM microphotographs of (a) HA, (b) HA/MoO$_x$ (II) and (c) HA/MoOx (III) nano-platforms. 3D surface plots of (d) HA, (e) HA/MoOx (II) and (f) HA/MoOx (III) nano-platforms. (g) ζ-potential of HA and HA/MoO$_x$ nano-platforms. (h) Elemental chemical microanalysis of HA and HA/MoOx nano-platforms obtained from X-ray energy-dispersive (EDX) spectroscopy; results are shown as Ca/P; Ca/Mo and Mo/P elemental ratio. (i) Ionic concentrations released from HA and HA/MoOx nano-platforms after incubation 10 days in PBS (pH = 7.4).

Infection on an implantable device surface is initiated by bacterial adhesion.[29] In general, because of the energetic difference between bacterial surfaces and aqueous environments, cells prefer to grow on solid substrates to which they anchor through non-specific interactions. If essential characteristics of bacteria are excluded, their adhesion performances are strongly determined by surface charge, wettability, topologies and roughness. Alterations in bacterial adhesion is the primary targeting step for developing antibacterial strategies.[3] Accordingly, as a first stage, bacterial cell / substrate local interaction and the possible disruption of the microorganism´s adsorption capacity due to

chemical, morphological and topographical cues of HA/MoO_x nano-platforms was inquired. In a previous work, [15] the microstructure and physical-chemical parameters of bare rod-like HA nanostructures networks and its nano-HA/MoO_x counterparts were widely characterized. Surface texture of HA and of HA/MoO_x samples exhibits a nano-structured network wrought by assemble of uniform rod-like nanoparticles, **figures 1a – 1c**. They shows positive values of R_{sk}, R_{ku} coefficients inferior than three and ζ-potentials of -18.4 ± 1.4 mV indicating the existence of a negative charged topography with a spiky profile at the nano-scale. Even though surfaces reveals relatively high peaks and low round valleys, **figures 1d – 1g**, no effects attributable to surface features against bacterial progression were detected.[15] However, a dependence, not linear though, between the antibacterial activity and the amount of MoO_x present was observed. Composition of HA/MoOx specimens were analysed, which is presented in **figure 1h**. Both untreated HA and HA /MoO_x derivatives, despite their different Ca/P; Ca/Mo and Mo/P configuration, **figure 1h**, behave as insoluble salts under physiological conditions (pH = 7.4, 1 bar, 37°C). We have confirmed that released ionic concentrations, **figure 1i**, were within the non-toxicity range [15] and, in addition, are not enough to alter the water accessibility to microorganisms. [30] Additionally, we have determined that pH of nutritive culture broth increases to a slightly alkaline value of 8.1 ± 0.2 after the material incorporation and the subsequent release of $[OH^-]$ = 0.47 mM, $[PO_4^{-3}]$ = 2.14 mM, $[HPO_4^{-2}]$ = 0.37 mM; this fact, far from killing bacteria should promote their proliferation.[31] Then, microenvironment modification in the surrounding area of the substrate or, even, in culture medium could not be associated with the experimentally found antibacterial effect. [15] According to the previous described results and having detected that, the HA/MoO_x nanostructured platforms have electron acceptor –OH vacancies defects, V_{OH},

directly related to MoO_x presence, antibiotic results was correlated to materials' electrogen induction skills. [15]

3.2 Electronic transference processes

Recognising that tested materials have electron acceptance capacity and having connected this capacity with bacterial annihilation, [15] the following stage was to validate these interactions and the mechanism by which bacteria transfer electrons to HA / MoO_x nano-platforms specimens. We have selected the cyclic voltammetric method to carry out our research because it is an expressly powerful tool to the study of electrode reaction mechanisms and of adsorbed species, including of biological substances throughout *in vivo* monitoring experiments.[32] Interfacial switch to reactivity and the manifestation of Faradaic processes was performed assessing the redox behaviour of surface sensitive probes as ascorbic acid, $Fe(CN)_6^{3-/4-}$, $Fe(H_2O)_6^{3+/2+}$ and dopamine. [33]

3.2.1 Faradaic processes at the HA / MoO_x nano-platforms interface

Electroactive performance, both in their redox potential (redox intensity component) and in their kinetic capacity (the ability of electrons to be transferred) of HA and HA/MoO_x nano-platforms electrodes (nano-PEs) were measured against the redox conversion of the benchmark $Fe(CN)_6^{-3/-4}$ probe; steady cyclic voltammograms (CVs) curves are shown in **figure 2a**. It can be noted, the clear formation of $Fe^{2+/3+}$ redox peaks in all tested electrodes indicating the characteristic reversible single-electron transfer processes. Highest and well-resolved Faradaic current peaks (i_p) suggest the occurrence of a net current flow controlled by diffusion processes at the electrode interface due to electron transfer reactions. Obtained i_p results are higher and comparable for MoO_x substituted-HA electrodes with slightly superior values contrasted to GCE reference, while a clear decrease was observed at undoped nano-HAE.

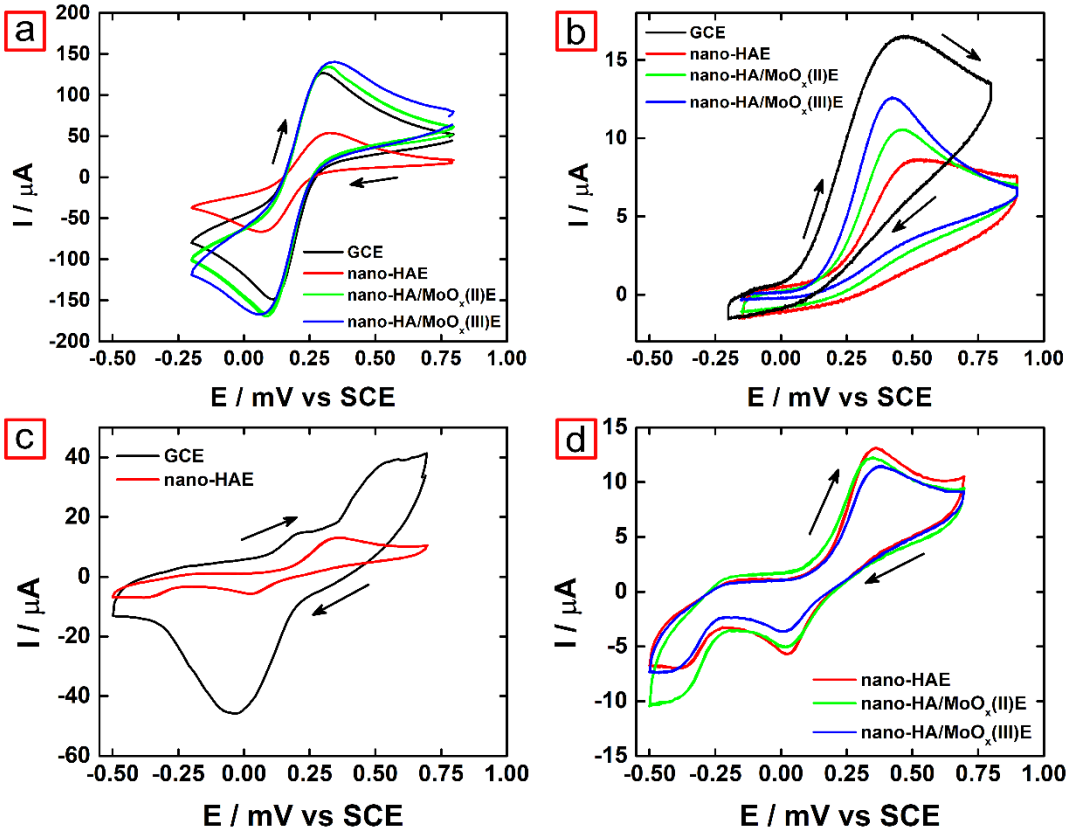

Figure 2. Steady cyclic voltammograms (CVs) curves of glassy carbon, nano-HA and modified nano-HA/MoO_x(II) and nano-HA/MoO_x(III) electrodes against the redox conversion of **(a)** $Fe(CN)_6^{-3/-4}$ couple; **(b)** ascorbic acid and **(c, d)** dopamine probes. CVs are recorded in a PBS solution (pH = 7.2; RT) at a scan rate of 50 mV s^{-1}. Saturated calomel electrode (SCE) was used as reference; arrows indicated scan direction.

The difference between the MoO_x substituted-HA electrodes is also evident in the behaviour of the ascorbic acid probe, **figure 2b**. Similarly than $Fe(CN)_6^{-3/-4}$ performance, peaks intensity increases with the switch of MoO_4^{2-} /PO_4^{3-} in the hexagonal HA crystal lattice. In this case, the anodic peak is associated with the irreversible transformation of Vitamin C in dehydroascorbic acid via a multistep process that involves the transfer of two electrons and one proton at neutral pH. At the operational conditions, ascorbic acid always displayed its characteristic single oxidation peak at the potential region between 0.0 and 0.8 V, demonstrating that nano-HA and MoO_x substituted-HA materials acted as electron acceptors. Neither for ascorbic acid nor $Fe(CN)_6^{-3/-4}$ probes, the shape of the CVs shows an influence of adsorption processes or the presence of oxides.[33] To evaluate the

possibility of adsorption of electroactive molecules from solution, we have investigated the behaviour of dopamine probe oxidation. Dopamine (3,4-dihydroxy phenethylamine, DA) is a catechol derivate which oxidized in a heterogeneous two-step mechanism that involves the transference of two electrons and two protons preceded by a strong adsorption step on the electrode surface,[33] **figures 2c** and **2d**.

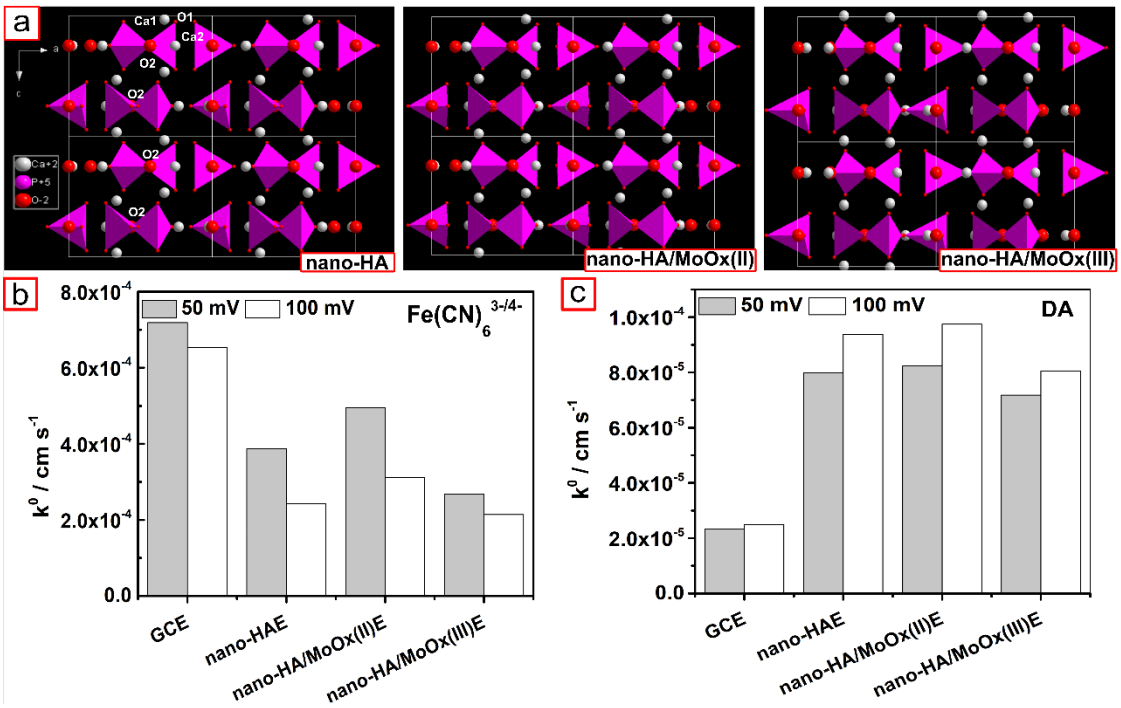

Figure 3. (a) Theoretical direct unit cell structures generated by *ab initio* methods of nano-HA, nano-HA/MoO_x(II) and nano-HA/MoO_x(III).[15] Variation of heterogeneous kinetic constant, k^0, obtained from CVs curves of modified GCE in 10 mM of **(b)** $Fe(CN)_6^{3-/4-}$ and **(c)** DA PBS solutions (pH = 7.4, RT).

DA oxidation is almost inhibited in the presence of nano-HAE surface compared to GCE, **figure 2c**, while no statistical significant differences among redox intensity components of nano-HAE and its MoO_x-substitute derivatives are observed, **figure 2d**. The oxidation of catechol analogues has been studied widely, due to the importance of catecholamine neurotransmitters and related compounds in biology. The catalytic effect was attributed to the presence of hydrogen bonding sites on the surface, in a process called "proton-assisted electron transfer". On bare GCE, catechol adsorbed via a noncovalent interaction

between the aryl ring π system and the graphitized regions of the surface to allow "autocatalysis" via self-hydrogen bonds. [33] On nano-HA, hydrogen bond interaction can be attained merely after contact with $-OPO_3^{3-}$ on the HA (0001) or with -OH on the HA (0001) planes.[34] Phosphate and hydroxyl ions are arranged in columns in twofold disorder with the O→ H direction pointing away from the mirror planes passing through the nearest coordinating calcium ions favouring adjacent hydroxyl ions, $OH \cdots OH \cdots OH$ interaction through a head-to-tail fashion, **figure 3a**. This arrangement favours the formation of H- bonds with dopamine and the electrochemical response of the probe, whenever they come into contact. Literature information suggest that oxygen-containing functional groups do not necessarily enhance DA adsorption and in some conditions have the opposite effect related with a restricted accessibility of the adsorption sites.[35] We hypothesize that DA electroactivity occurs only after interaction with $-OPO_3^{3-}$ or -OH groups on the nano-HA electrodes; the restriction in their accessibility is the cause of the significant reduction in Faradaic current peaks compared with GCE. To attain a deeper conclusion about the mechanism of interaction, we have analysed the electronic transference kinetic process by Randles–Ševčik equation. The catalytic mechanism, for a given redox system, involving a particular surface group, is unlikely to be important if the heterogeneous rate constant, k^0, is not affected. Furthermore, rate constants are structure-dependent of the local density of states (DOS) at the Fermi level. [36] Heterogeneous rate constant results obtained for $Fe(CN)_6^{3-/4-}$ probe are shown in **figure 3b**; an about of 50 % of decrease for nano-HAE and MoO_x-substituted derivatives are observed compared to the vitreous carbon used as control. Evaluating the calcium phosphate materials, an increase in the transfer rate is detected in the following sequence: nano-HA/MoO_x(II)E > nano-HAE > nano-HA/MoO_x(III)E. Regarding to dopamine probe, in contrast, a 350 % of increase of k^0 values compared to the control (GCE), is

noted; maximum value corresponds to nano-HA/MoO_x(II)E, **figure 3c**. An equivalent behaviour was prior detected for ascorbic acid, where k^0 was strongly influenced by the MoO_4^{2-}/ PO_4^{3-} substitution, acquiring a maximum value for the HA/MoOx (II)E where no extra MoO_4^{2-} - crystalline phases are present. Electronic transference rate results were contrasted with optical band gaps energies, E_g, whose values were determined in a previous work[15] and discussed in terms of the density of electronic states.

-Please, insert **table 2**, here-

Nano-HA, $(Ca^{+2})_{9.12}(PO_4^{-3})_{5.12}(HPO_4^{-2})_{0.88}(OH^-)_{1.12}$, and nano-HA/$MoO_x$(II) samples exhibited E_g values of 5.87 ± 0.14 eV and 5.65 ± 0.21 eV respectively. Structural order straight increases the band gap energies, so an excitation energy of about 1.5 eV inferior to defect-free HA lattice (7.7 ± 0.2 eV [37]) implies a transition involving at least one bound state located in the gap. Replacement of PO_4^{3-} by MoO_4^{2-} in the original HA structure generates slightly distortions of distance and angles between atomic positions in the crystal lattice, **table 2.** These are connected with the creations of vacancies, inter-nodes and other defects that generates a redistribution of the electrons in the occupied / unoccupied electronic energy levels. In particular for nano-HA/MoO_x(II), experimental data agrees with reported literature values observed for the OH-vacancy HA cell ($E_g \approx$ 5.5 eV [38]), so we assume that its structure mostly accords with the latter. Nano-HA/MoO_x(III) specimen, conversely, presented an E_g = 4.77 ± 0.11 eV, associated with the presence of powellite phase ($E_g \approx$ 4.70 eV [39]) displaying multi-phonon and multi-level processes within the band gap that interfere with the OH-vacancies, V_{OH}. It is tempting to attribute enhanced electron-transfer kinetics of HA/MoO_x(II) specimen to the presence of V_{OH} defects. The latter mentioned periodic $OH \cdots OH \cdots OH$, hydrogen bridge chain in the nano-HA structure, carries an anti-bonding σ* character, suggesting the formation of

a conductive 1D-ice phase.[37] The electronic band structure of nano-HA and nano-HA/MoO_x (II) with OH-vacancy defects, V_{OH}, differs from that of bulk, only by the presence of an additional semi-occupied defect-related band close to mid-gap. This suggests that V_{OH} can donate an electron (leaving the defect band empty) or accept an electron (filling up the defect band) manifesting a unique electroactive effect. Computed values of torsion angle between periodic $OH \cdots OH \cdots OH$, hydrogen bridges are equal to 180° in all tested material, **table 2**. Considering the assumption that the electrochemical activity of the DA probe is catalysed by its specific adsorption on $OH \cdots OH \cdots OH$, sites, it is logical to think of similar behaviour for nano-HA modified electrodes. For outer-sphere electron transfer reaction, ascorbic acid and $Fe(CN)_6^{3-/4-}$ probes that not require adsorption, the "site" must include an electronic perturbation of the surface.[40] As we have previously mentioned, several levels or the narrow energy band in the middle of the forbidden band gap, E_g, as occurs for nano-HAE and MoO_x-derivatives, must belong directly to the OH-vacancy, which may exist at higher concentrations in HA surface layer. [38] Such intrinsic point defects generate localized electronic states that increase the density of electronic states (DOS) near the Fermi level, making electron transfer of ascorbic acid and $Fe(CN)_6^{3-/4-}$ probes directly proportional to its increase in agreement with our k^0 values, **figure 3b**.

3.2.2 Faradaic processes after bacteria adsorption at electrode interfaces

In the previous section we analysed the data and the electrochemical reactions that take place at the electrode/solution interface, here, in the case of electroactive microbial adsorption, the processes occur between the adsorbed bacterial film (ABF) and the electrode interface; however, the ABF could be considered part of the electrode, **scheme 1a**.[41] Electroactive performance of *Staphylococcus aureus* and *Pseudomona aeruginosa*

strains adsorbed on glassy carbon, HA and HA/MoO_x nano-platforms electrodes were measured against the redox conversion of $Fe(CN)_6^{-3/-4}$ probe; steady cyclic voltammograms (CVs) curves were shown in **figure 4**. In all tested systems, shapes of CVs indicate that Faradaic processes occur, however these largely depend on the electrode material and on the presence of bacterial strains indicating microbial participation in the events that occur at the electrode interface and the microbial capacity for extracellular electron transfer (EET)-driven electron exchange. [42]

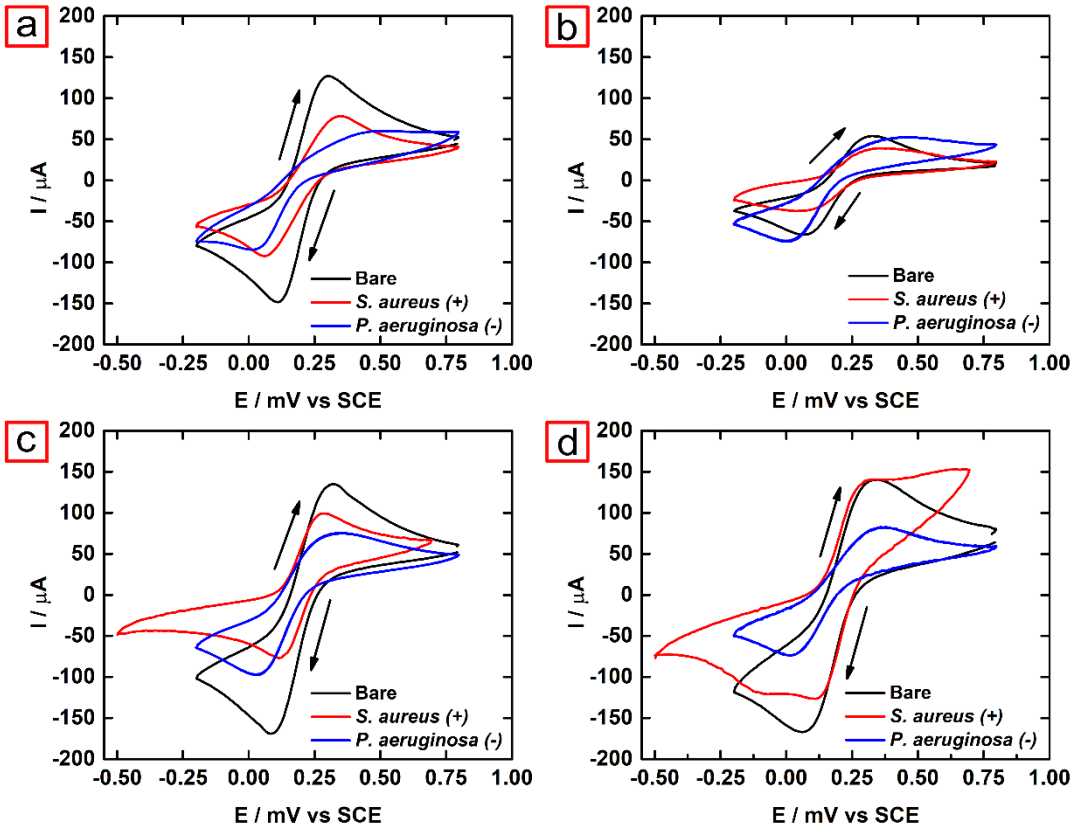

Figure 4. Steady cyclic voltammograms (CVs) curves of **(a)** glassy carbon (GC) and modified **(b)** nano-HA, **(c)** nano-HA/MoO_x(II) and **(d)** nano-HA/MoO_x(III) electrodes after *Staphylococcus aureus* and *Pseudomona aeruginosa* adsorption. CVs are recorded for 10 mM $[Fe(CN)_6]^{3-/4-}$ redox couple PBS solution (pH = 7.2; RT) at a scan rate of 50 mV s^{-1}. The arrows indicated the scan direction; saturated calomel electrode was used as reference.

Precise $[Fe(CN)_6]^{3-/4-}$ redox couple oxidation and reduction peaks are observed after the adsorption of *Staphylococcus aureus*, while for *Pseudomona aeruginosa* the typical s-

shape curve was evident only in PA / nano-HA/MoO_x(II) and PA / nano-HA/MoO_x(III) electrodes. Except for nano-HAE, there is a reduction of Faradaic current peaks intensity (i_p) due to bacteria / material interaction and this effect is further evident for *Pseudomona aeruginosa* than for *Staphylococcus aureus* adsorption. At this point, microorganisms can exert different effects as it is shown in **scheme 1b**: (1) they can participate in redox events by transferring their metabolic electrons, e_{met}^-, to the probe acting as active site; (2) they can transfer their e_{met}^- to the electrode material on which they are adsorbed; or they can simply restrict access to the electroactive sites of the electrode material (3).

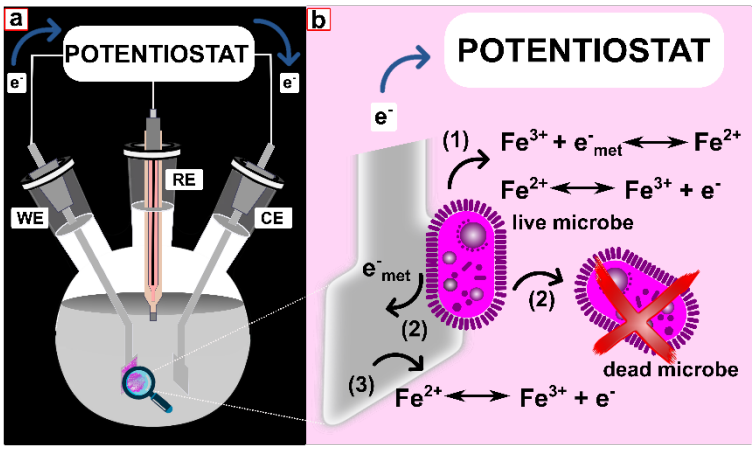

Scheme 1. (a) Three-electrode electrochemical cell, containing a working electrode (WE: GCE/bacteria; nano-PEs/bacteria), a counter electrode (CE: platinum wire) and a reference electrode (RE: SCE, + 0.241 vs. NHE). **(b)** Mechanism of bacteria / nano-PEs surface interactions; CAs were recorded throughout 24 hours at RT checking the redox conversion of $Fe^{+2/+3}$ probe in a PBS solution containing 50 µM of ferrous sulfate, 100 µM of ferric sulfate and 100 mM Glucose. (1) Live microbes act as active site transferring their metabolic electrons, e^-_{met}, to redox probe. (2) Live microbes transfer e^-_{met} to electrode following by their dead. (3) Electrode active sites transfer e^- to redox probe.

It was determined that bacteria are uniformly adsorbed and in the same amount regardless of the type of material that constitutes the electrode, **section 2.3.3, table 1**. Accordingly, if microbes had their own role as electroactive sites, this would be equally evident at all electrodes that does not agree with our experimental data, **figure 4**. Furthermore, no

additional peaks associated to multiple redox centres exposed on the surfaces were detected, **figure 4**. Once route (1) of bacterial action has been ruled out, we focus on routes (2) and (3). Route (2) clearly increases the electronic transfer to the material and the electroactive response, while route (3) decreases it. In both cases, there is a specificity of bacterial interaction with electrode components, which is in completely accord with our experimental data. Similar to the previous section, the potential difference between the oxidation and reduction peaks, ΔE_p, was taken as an indicator of the heterogeneous electron transfer rate. When the value of $\Delta E_p/z$ is close to 59 mV/z, where z is the number of electrons exchanged by the redox couple, the system is completely reversible. The transfer of electrons at the interface between the electrode and the electrolyte occurs at rates high enough so that equilibrium is respected, as dictated by the Nernst equation, at the electrode/electrolyte interface and the maximum anodic and cathodic potentials are not change with scan rate. All tested systems exhibited $\Delta E_p > 59$ mV, $z = 1$, that varied with scan rate demonstrating a quasi-reversible delayed electron transfer process, **table 3**. Despite the presence of bacteria, processes follow a typical Randles–Sevcik behaviour, where each bacteria modified electrode current peak, in both the oxidation and reduction branches of the voltammograms, varied linearly with the square root of the scan rate. This means that all electrodes mimics the electrochemical characteristics of a solid planar macro-electrode, where the diffusion layers originated at the bacteria adsorbed platforms are overlapped resulting in a semi-infinite planar diffusion controlled process.

- Please, insert table 3, here -

Comparing the materials constituents of electrodes, it is observed that, after adsorption of both types of bacteria strain, the electronic transfer is faster for the MoO_x substituted nano-HA electrodes. Contrasting the adsorbed bacteria, there is an augment of k^0 values after *Staphylococcus aureus* interaction. Heterogeneous rate constant for the SA / nano-

HA/MoO_x (II)E system was about 1.5; 2.0 and 2.5 times superior than bare electrodes of GC, nano-HA/MoOx (II) and nano-HA respectively. Furthermore, it is 4 and 5.7 times superior to SA / GCE and SA / nano-HAE systems respectively. SA / nano-HA/MoO_x (III)E system shows a k^0 value that is 1.5 and 2 times superior than bare nano-HAE and nano-HA/MoO_x(III)E respectively, while inferior than SA / nano-HA/MoO_x (II)E system. After adsorption of *Pseudomona aeruginosa,* kinetic of electronic transfer is drastically reduced for all systems in comparison with bare electrodes, denoting a clear interference of bacteria with the material electroactive sites. However, PA / nano-HA/MoO_x (II)E and PA / nano-HA/MoO_x (III)E systems show an increment in k_0 values contrasted with those systems containing GCE and nano-HAE demonstrating that despite restricting access to the active sites of HA, the switch of MoO_4^{2-} /PO_4^{3-} in the original hexagonal nano-HA crystal lattice causes a positive electroactive interaction with microorganism. Summarizing, results indicate a clear modification of redox behaviour due to de bacteria/material interaction and the increase in the electroactive response of the material (increment on k^0) is associated with some type of EET with adsorbed microbes. Confirmation of route (2) of scheme 1, a real extracellular electron transference between microorganisms and the material constituting the working electrode, was performed after chronoamperometry (CA) examination. Bacteria EET implies a physical conductive contact, which allows electron transfer across cell membranes to external solid materials, i.e., electrodes or minerals, thus, chronoamperometry is a powerful tool for untangling the effects of electrode potential and time, which are convoluted in the previous shown cyclic voltammetric measurements. In CA experiments, the current potential of CG, nano-HA, nano-HA/MoOx(II) and nano-HA/MoOx(III) previously exposed to microorganisms was stepped against a reference standard electrode giving an electric response that was recorded over time; results are shown in **figure 5**. Always a positive current was

registered, confirming that microorganisms transfer electrons to the working electrode (anodic reactions). [43] The applied potential is constant (0.2 V) and current intensity data are expressed for bacteria colony forming units (CFU), therefore, the increase in the current magnitude that is observed on certain intervals is a consequence of bacterial film electroactive interaction. *Staphylococcus aureus* is a Gram-positive bacterium; as such, it has a thick, non-electron conducting cell wall of 6 to 18 peptidoglycan units layer and is believed to have weak extracellular electron transport activity, [42] which agrees with lower current values in the chronoamperogram than those observed for *Pseudomonas aeruginosa,* **figure 5**.

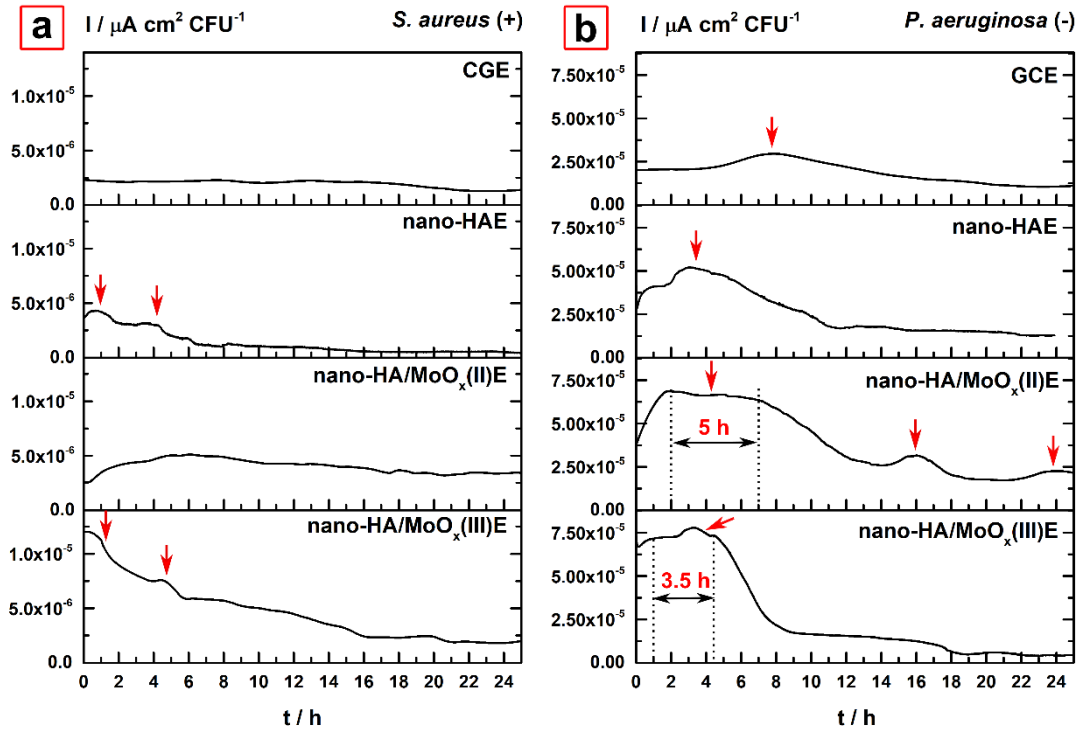

Figure 5. Chronoamperometry (CA) registered for glassy carbon and modified nano-HA, nano-HA/MoOx(II) and nano-HA/MoOx(III) electrodes after (a) Staphylococcus aureus and (d) Pseudomona aeruginosa adsorption. CA are recorded for 10 mM $[Fe(H_2O)_6]^{2+/3+}$ probe in PBS solution (pH = 7.2; RT) at a fixed voltage of 0.2 V. Current intensity peaks are signed with red arrows.

Due to the structural characteristics of the cell envelope, Gram-positive bacteria generally is considered incapable of EET without presence of diffusible mediators, accordingly,

literature investigations reported the involvement of several cell wall-associated multiheme c-type cytochromes in their EET processes.[44] Cytochromes are essential electron carriers and key players in the EET processes of the model Gram-negative organisms like *Geobacter* or *Shewanella*, [42] however in Gram-positive bacteria normally cytochromes are involved in the respiratory chain and is likely associated with the inner cytoplasmic membrane. The presence of multiheme cytochromes exposed on the cell surface is an unusual property to Gram-positive bacteria, but it could be possible if the cell wall is altered due to interaction with the electrode material. Under those conditions, electrons can flow through an unidentified protein or through the cytochromes of the periplasmic hydrogenase subunits in the outer membrane. In a previous work,[15] we have confirmed that the leakage of cytoplasmic constituents was boosted in the presence of nano-HA and their HA/MoO_x derivatives, under the same conditions, current peaks appear that are not seen when the bacteria is in contact with the vitreous carbon, **figure 5a**. A greater current intensity are observed after *Staphylococcus aureus* interaction with nano-HA/MoOx (II)E and nano-HA/MoOx (III)E, which also explains the increment of electronic transfer rate previously detected, **table 3**. *Pseudomonas aeruginosa* is a Gram-negative microorganism that secretes and involves phenazines in its EET; the production of this compound also promotes tolerance to antibiotics and metabolic heterogeneity in biofilms. [45] Secretion of extracellular electron shuttles, phenazines, matched with the greater current values registered in chronoamperograms, **figure 5b**. It was observed a clear difference among chroamperograms recorded against substituted nano-HA electrodes compared with GCE and nano-HAE. In the case of CGE and nano-HA, a peak current is recorded while in the presence of substituted nano-HAEs current intensity shows superior keep constant over 3.5 – 5 hours, denoting a sustained interaction with the

electron intermediaries. Maximum contact, 5 hours, was registered with nano-HA/MoOx (II)E explaining the highest previously detected electronic transfer rate value, **table 3**.

3.3 Ultrastructural changes of microorganism by MoO_x-hydroxyapatite nano-platforms

Intracellular structural changes in bacteria cultured in absence and in presence of MoO_x-hydroxyapatite nano-platforms are examined by TEM and representative cross-sectional area images are shown in **figure 6.**

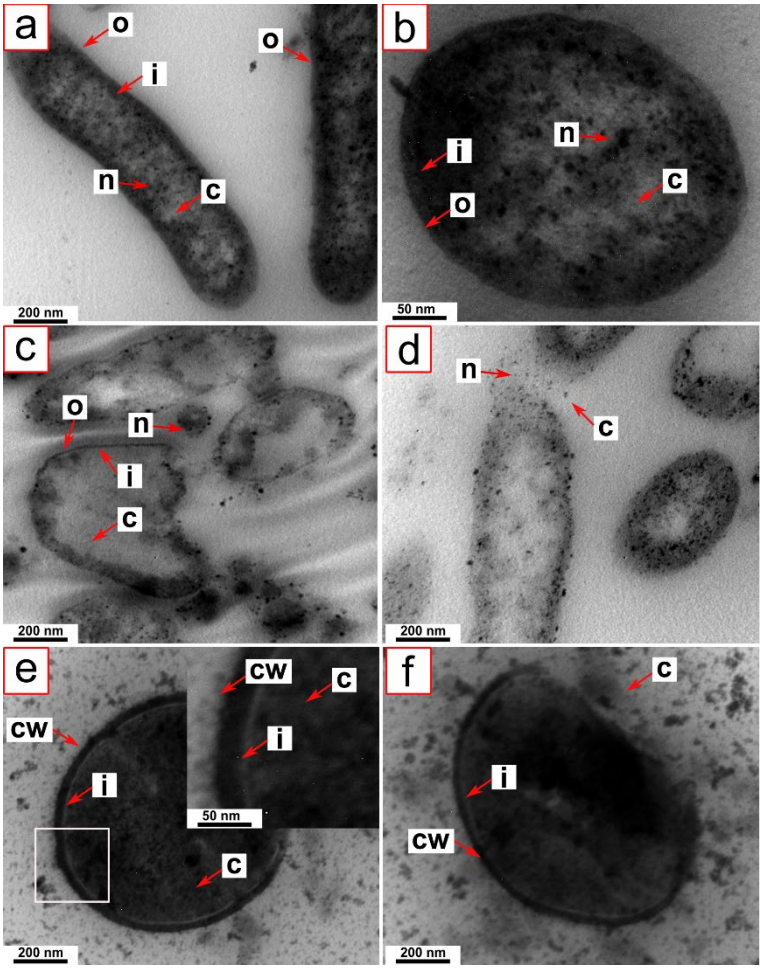

Figure 6. Bacterial ultrastructure observed by TEM. Longitudinal and transversal cross-section of *P. aeruginosa* after culturing alone **(a, b)** and in the presence of nano-HA/MoOx(II) **(c, d)**. Transversal cross-section of *S. aureus* after culturing alone **(e)** and in the presence of nano-HA/MoOx(II) **(f)**. Cell wall (cw), internal cytoplasmic membrane (i), outer membrane (o) cytoplasm (c) and nucleolus (n) are signed with red arrows.

Figures 6a and **6b** display longitudinal and transversal cross-sectional areas of *Pseudomona aeruginosa* cultured in the absence of materials. It can be observed that cells maintained their rod-like shapes and morphological integrity; characteristic internal cytoplasmic membrane and its second membrane, the outer membrane that forms the exterior of the gram-negative bacteria cell, are also appreciated. Contrary, in the presence of nano-HA/MoO_x(II) material, distribution of cytoplasmic components became no uniform, the membrane structure of treated cells became smoother and thinner than that of the untreated cells; in selected areas, the cytoplasm emerged from broken parts of cytoplasmic membrane. In addition, it can be appreciated several rough structures, perceived as black spots, located on the cell surfaces and outside cells, which can be identified as cellular constituents leaking from bacteria after material interaction, **figures 6c** and **6d**. A similar effect can be appreciated for *Staphylococcus aureus,* **figures 6d** and **6e**, demonstrating that materials are also effective to disrupt cell wall of Gram-positive bacteria leading the permeation of cellular compounds from treated cells. The impact of the nano-HA/MoO_x(II) material on the ultrastructure of *P. aeruginosa* and *S. aureus* cells was mainly focused on surface assembly: membrane rupture and leakage of cytoplasmic components; which agrees with our observations that its effect on microbial kill occurs after direct interaction and not by effects on its surrounding environment. The cytoplasmic membrane contains many different protein species that take part in many metabolic processes, including electron transport and oxidative phosphorylation, protein synthesis, DNA replication, secretion of macromolecules, and synthesis of cell wall components; its disruption results in cell death. A 85 % leakage of cytoplasmic constituents was confirmed for nano-HA and nano-HA/MoOx(II) samples, while no reducing sugar escape was register in control experiments.[15] TEM observations are

similar to the ultrastructural changes in bacteria exposed to TiO_2 nanotubes platforms detected by Wang *et al.* [16, 17]. The authors state that active electrons from the respiration chain of microorganisms are transferred to materials, in an enhanced electron transfer mechanism, rather than being actively donated by bacteria to energy generation that die from electron loss. On basis of a similar charge transfer approach, Zhang et al.[18] also demonstrated that Cu-bearing stainless steel materials promote an effective contact to induce bacteria-killing. In attendance, the cathode electrons generated by the potential difference of the material microdomain caused proton depletion in the bacterial cells, thus perturbing the respiratory chain of the bacterial cells. The proposed mechanisms are in agreement with our electrochemical experimental results, section 3.2. We have confirmed samples biocompatibility analyzing viability and morphology of rat primary osteoblast; results long-established that the charge transfer approach is not operative in the presence of eukaryote cells.[15] Since eukaryotic cells carry out their respiratory chain within mitochondria, compartmentation of electrons do not allow their transference. Achievement of positive biocompatibility results for all tested MoO_x-hydroxyapatite nano-platforms reaffirms the concept of a mechanism of electron transfer by direct contact between the prokaryote cells and the material leading to his death, **scheme 1b**.

CONCLUSION

The charge transfer theory of bacterial killing was investigated for MoO_x – substituted phosphate based nanoplatforms and a type of extracellular electron transfer (EET) was observed from microbial cells to materials' surfaces conducting to their death. First, electroactive performance of HA and HA/MoOx nano-platforms electrodes (nano-HAE, nano-HA/MoOx(II)E and nano-HA/MoOx(III)E) were determined against the redox conversion of surface sensitive probes as ascorbic acid, $Fe(CN)_6^{3-/4-}$, $Fe(H_2O)_6^{3+/2+}$ and

dopamine. In all experiments, high and well-resolved faradaic peaks were obtained that suggest the occurrence of a net current flow controlled by diffusion processes at the electrode interface due to electron transference reactions. Interfacial switch to reactivity and the manifestation of Faradaic processes are related to the switch of MoO_4^{2-} /PO_4^{3-} in the original hexagonal nano-HA crystal lattice and the extent of OH-vacancies, V_{OH} defects. V_{OH} defects increase the density of electronic states (DOS) near the Fermi level, making electron transfer of ascorbic acid and $Fe(CN)_6^{3-/4-}$ probes directly proportional to its rise and conditioning the electroactivity of dopamine probe that occurs only after interaction with -OPO_3^{3-} or -OH groups. Electronic transference rate increased in the following sequence: nano-HA/MoO_x(II)E > nano-HAE > nano-HA/MoO_x(III)E, and always the substrate acted as electron acceptors. Following, Faradaic processes are analysed after *Staphylococcus aureus* and *Pseudomona aeruginosa* adsorption at electrode interfaces. Potential difference between the oxidation and reduction peaks, ΔE_p was always superior to 59 mV and varied with scan rate demonstrating a quasi-reversible delayed electron transfer process following the typical Randles–Sevcik behaviour. Comparing the materials constituents of electrodes, it is observed that, after adsorption of both bacteria strain, the electronic transfer is faster for the MoO_x substituted nano-HA electrodes. Contrasting the adsorbed bacteria, there is an augment of k_0 values after *Staphylococcus aureus* that exceeds the values obtained from the control (GC) and bare electrodes. *Pseudomona aeruginosa*-containing systems shows a clear decrease of electronic transfer rate, nevertheless k_0 values for *Pseudomona aeruginosa* / MoO_x substituted nano-HA electrodes are superior compared with control and unsubstituted nano-HA electrodes. Chronoamperometry (CA) examination revealed different profiles because of a bacterial-specificity interaction, however in both *Staphylococcus aureus*- and for *Pseudomona aeruginosa*-containing systems a positive current was registered

confirming that microorganisms transfer electrons to the working electrode (anodic reactions). After inspection of microorganisms ultrastructural changes an effective disruption of cytoplasmic membrane and the permeation of cellular compounds from treated cells were noted after their culture in presence of materials. The impact of tested materials on both bacterial strains surface structure, while not on prokaryote cells, in addition to the faradaic processes registered both in the presence and in the absence of bacteria, validate the presence of some type of EET that alter microorganism's metabolic progression until their death. These processes had not been reported for MoO_x – substituted phosphate based nano-platforms and contribute to increasing the knowledge of electroactive building blocks for new materials against bone infections.

ACKNOWLEDGEMENTS. The authors acknowledge the financial support of Universidad Nacional del Sur (UNS, PGI 24/Q092), Ministerio de Ciencia e Innovación (PID2019- 805 111327GB-100) and Xunta de Galicia (ED431B 2022/36). DP thanks CONICET for his fellowship. JMS and PVM are researchers of CONICET.

REFERENCES

1. K. Chae, W. Y. Jang, K. Park, J. Lee, H. Kim, K. Lee, C. K. Lee, Y. Lee, S. H. Lee and J. Seo, *Science Advances*, 2020, **6**, eabb0025.
2. K. L. Urish and J. E. Cassat, *Infection and immunity*, 2020, **88**, e00932-00919.
3. W. Li, E. S. Thian, M. Wang, Z. Wang and L. Ren, *Advanced Science*, 2021, **8**, 2100368.
4. L. M. Pezzanite, L. Chow, V. Johnson, G. M. Griffenhagen, L. Goodrich and S. Dow, *Veterinary Surgery*, 2021, **50**, 858-871.
5. L. Chen, L. Shao, F. Wang, Y. Huang and F. Gao, *RSC advances*, 2019, **9**, 10494-10507.
6. N. Karamat-Ullah, Y. Demidov, M. Schramm, D. Grumme, J. Auer, C. Bohr, B. Brachvogel and H. Maleki, *ACS Biomaterials Science & Engineering*, 2021, **7**, 4545-4556.
7. X.-Y. Zhang, Y.-Q. Zhao, Y. Zhang, A. Wang, X. Ding, Y. Li, S. Duan, X. Ding and F.-J. Xu, *Biomacromolecules*, 2019, **20**, 4171-4179.
8. B. Jia, X. Du, W. Wang, Y. Qu, X. Liu, M. Zhao, W. Li and Y.-Q. Li, *Advanced Science*, 2022, **9**, 2105252.
9. H. Wei, J. Cui, K. Lin, J. Xie and X. Wang, *Bone research*, 2022, **10**, 1-19.
10. M. M. Fernandes, D. M. Correia, C. Ribeiro, N. Castro, V. Correia and S. Lanceros-Mendez, *ACS applied materials & interfaces*, 2019, **11**, 45265-45275.
11. L. Leppik, K. M. C. Oliveira, M. B. Bhavsar and J. H. Barker, *European Journal of Trauma and Emergency Surgery*, 2020, **46**, 231-244.
12. N. C. Andrés, N. L. D'Elía, J. M. Ruso, A. n. E. Campelo, V. L. Massheimer and P. V. Messina, *ACS applied materials & interfaces*, 2017, **9**, 15698-15710.
13. N. C. Andrés, J. M. Sieben, M. n. Baldini, C. H. Rodríguez, A. n. Famiglietti and P. V. Messina, *ACS applied materials & interfaces*, 2018, **10**, 19534-19544.
14. N. L. D'Elía, C. Mathieu, C. D. Hoemann, J. A. Laiuppa, G. E. Santillán and P. V. Messina, *Nanoscale*, 2015, **7**, 18751-18762.
15. D. Placente, J. M. Ruso, M. Baldini, J. A. Laiuppa, J. M. Sieben, G. E. Santillán and P. V. Messina, *Nanoscale*, 2019, **11**, 17277-17292.
16. G. Wang, H. Feng, A. Gao, Q. Hao, W. Jin, X. Peng, W. Li, G. Wu and P. K. Chu, *ACS Appl. Mater. Interfaces*, 2016, **8**, 24509-24516.
17. G. Wang, H. Feng, L. Hu, W. Jin, Q. Hao, A. Gao, X. Peng, W. Li, K. Y. Wong, H. Wang and Z. Li, 2018, **9**, 2055.
18. X. Zhang, C. Yang and K. Yang, *ACS Applied Materials & Interfaces*, 2020, **12**, 361-372.
19. S. Rtimi and J. Kiwi, *Catalysts*, 2021, **11**, 201.
20. E. Gadelmawla, M. M. Koura, T. M. Maksoud, I. M. Elewa and H. Soliman, *Journal of materials processing Technology*, 2002, **123**, 133-145.
21. C. A. Schneider, W. S. Rasband and K. W. Eliceiri, *Nat. Methods*, 2012, **9**, 671.
22. R. Hunter, *New York, USA*, 1981.
23. D. Placente, L. A. Benedini, M. Baldini, J. A. Laiuppa, G. E. Santillán and P. V. Messina, *Int. J. Pharm.*, 2018, **548**, 559-570.
24. D. Clark, *Canadian Journal of Microbiology*, 1965, **11**, 407-413.
25. J. Ho, T. Tumkaya, S. Aryal, H. Choi and A. Claridge-Chang, *Nature Methods*, 2019, **16**, 565-566.
26. P. Krishnaveni and V. Ganesh, *Scientific Reports*, 2021, **11**, 7663.
27. C. Liu, T. Sun, Y. Zhai and S. Dong, *Talanta*, 2009, **78**, 613-617.
28. A. J. Bard and L. R. Faulkner, *Journal*, 2001.
29. M. Ribeiro, F. J. Monteiro and M. P. Ferraz, *Biomatter*, 2012, **2**, 176-194.
30. W. M. Sattley and M. T. Madigan, *eLS*, 2001, 1-10.
31. L. Bennison, C. Miller, R. Summers, A. Minnis, G. Sussman and W. McGuiness, *Wound Practice & Research: Journal of the Australian Wound Management Association*, 2017, **25**, 63-69.

32. A. J. Bard, L. R. Faulkner and H. S. White, *Electrochemical methods: fundamentals and applications*, John Wiley & Sons, 2022.
33. R. L. McCreery, *Chemical Reviews*, 2008, **108**, 2646-2687.
34. W. Xia, C. Lindahl, J. Lausmaa and H. Engqvist, *Advances in biomimetics*, 2011, **20**, 429-452.
35. D. L. Swinya, D. Martín-Yerga, M. Walker and P. R. Unwin, *The Journal of Physical Chemistry C*, 2022, **126**, 13399-13408.
36. J. M. Sieben, A. Ansón-Casaos, F. Montilla, M. T. Martínez and E. Morallón, *Electrochimica Acta*, 2014, **135**, 404-411.
37. L. A. Avakyan, E. V. Paramonova, J. Coutinho, S. Öberg, V. S. Bystrov and L. A. Bugaev, *The Journal of Chemical Physics*, 2018, **148**, 154706.
38. A. V. Bystrova, Y. D. Dekhtyar, A. I. Popov, J. Coutinho and V. S. Bystrov, *Ferroelectrics*, 2015, **475**, 135-147.
39. J.-W. Yoon, C.-J. Choi and D. Kim, *Materials transactions*, 2011, 1102211311-1102211311.
40. M. T. McDermott and R. L. McCreery, *Langmuir*, 1994, **10**, 4307-4314.
41. F. Harnisch and S. Freguia, *Chemistry, an Asian journal*, 2012, **7**, 466-475.
42. G. Pankratova, L. Hederstedt and L. Gorton, *Analytica Chimica Acta*, 2019, **1076**, 32-47.
43. M. O. Yee, J. Deutzmann, A. Spormann and A.-E. Rotaru, *Nanotechnology*, 2020, **31**, 174003.
44. H. K. Carlson, A. T. Iavarone, A. Gorur, B. S. Yeo, R. Tran, R. A. Melnyk, R. A. Mathies, M. Auer and J. D. Coates, *Proceedings of the National Academy of Sciences*, 2012, **109**, 1702-1707.
45. S. H. Saunders, E. C. M. Tse, M. D. Yates, F. J. Otero, S. A. Trammell, E. D. A. Stemp, J. K. Barton, L. M. Tender and D. K. Newman, *Cell*, 2020, **182**, 919-932.e919.